

Tracking the variation of entanglement Rényi negativity : A quantum Monte Carlo study

Yi-Ming Ding,^{1,2} Yin Tang,^{1,2} Zhe Wang,^{1,2} Zhiyan Wang,^{3,1,2} Bin-Bin Mao,⁴ and Zheng Yan^{1,2,*}

¹*Department of Physics, School of Science and Research Center for Industries of the Future, Westlake University, Hangzhou 310030, China*

²*Institute of Natural Sciences, Westlake Institute for Advanced Study, Hangzhou 310024, China*

³*State Key Laboratory of Surface Physics and Department of Physics, Fudan University, Shanghai 200438, China*

⁴*School of Foundational Education, University of Health and Rehabilitation Sciences, Qingdao 266000, China*

Entanglement entropy has been a powerful tool for analyzing phases and criticality in pure ground states via quantum Monte Carlo (QMC). However, mixed-state entanglement, relevant to systems with dissipation, finite temperature, and disjoint regions, remains less explored due to the lack of efficient numerical methods. In this work, we present a practical and easy-to-implement QMC method within the reweight-annealing framework, enabling efficient computation of the entanglement Rényi negativity (RN) by tracking its variation along given parameter paths. This method is scalable, parallelizable, and well-suited for high-dimensional and large-scale simulations. Applying it to diverse scenarios—including 1D and 2D systems, ground and thermal states, and bipartite and tripartite partitions, not only the information of the underlying conformal field theory is achieved, but the role of entanglement in quantum and thermal phase transitions is revealed.

Introduction.— The increasing connection between condensed matter physics and quantum information science have significantly deepened our understanding of quantum many-body behaviors. Beyond the conventional Landau-Ginzburg-Wilson framework of symmetry breaking and phase transitions [1, 2], quantum entanglement and other intricate microcosmic degrees of freedom have become central in explaining various exotic emergent phenomena [3–5]. In a bipartite composite system, the entanglement of a pure ground state can be quantified by *entanglement entropy* (EE), which captures universal information of the system including critical behaviors [6–9], continuous symmetry breaking [10–13], the underlying conformal field theory (CFT) [14–18] and topological order [19–23]. However, EE fails as a measure of entanglement in mixed states, which frequently arise in many-body physics, such as in finite-temperature Gibbs states, systems with disconnected partitions, and open quantum systems [2, 4, 24]. Quantifying mixed-state entanglement remains difficult both analytically and numerically, as computing most existing measures requires complex optimization over the full Hilbert space [25–28].

The *entanglement logarithmic negativity*, referred to as *negativity* in this letter, is an important entanglement monotone for mixed states that can be computed without requiring optimization procedures [29–38]. Given a bipartite composite system $A \cup B$ in state ρ , the negativity that quantifies the entanglement between A and B is defined as $\mathcal{E} := \ln \|\rho^{T_B}\|$, where T^B denotes the partial transpose operating on subsystem B , and $\|\cdot\|$ is the trace norm, which sums over all absolute values of the eigenvalues of ρ^{T_B} . According to the positive partial transpose (PPT) criterion [39–41], a nonzero value of negativity indicates the existence of entanglement. While the converse

does not always hold, building on the PPT criterion, negativity has been demonstrated as a powerful tool for characterizing mixed-state entanglement [42–59]. However, for general many-body systems, it is highly challenging to accurately determining the full spectrum of ρ^{T_B} to compute negativity. Instead, the moments $\text{tr}[(\rho^{T_B})^n]$, where $n \geq 1$ is an integer, are more tractable [42–44, 60–63]. Particularly, the *Rényi negativity* (RN), a Rényi version of negativity, has emerged as an important quantity for studying mixed-state entanglement [62, 64–67]. It is defined as

$$R_n(\rho) := -\ln \frac{\text{tr}[(\rho^{T_B})^n]}{\text{tr}(\rho^n)} \quad (1)$$

Although RN is not an entanglement monotone as it may increase under local operations and classical communications [65], it can reflect many important properties of entanglement just as the negativity. For instance, it obeys the area law and the area-law coefficient is singular at the finite temperature critical point [64, 66, 68, 69]. From the perspective of numerical computation, RN and negativity share a relationship analogous to that between Rényi EE and von Neumann EE, with the former being more tractable.

In recent years, some numerical approaches have been developed to calculate RN or the moments [61, 62, 64, 66, 70]. However, efficient algorithms for exploring how RN varies with system parameters in large-scale and high-dimensional settings remain scarce, as existing methods typically compute RN at only a single parameter point per run, making it computationally expensive to obtain a full RN curve. Particularly for large-scale interacting spin/boson systems, there are few quantum Monte Carlo (QMC) works [71, 72], mainly because the incremental trick commonly used in calculating Rényi EE [11, 73, 74] becomes much more complex and difficult in the case of RN, since the lowest order of nontrivial RN is third and the boundary condition of imaginary time is twisted.

* zhengyan@westlake.edu.cn

Therefore, developing an efficient QMC algorithm that is both easy to implement and capable of accurately computing RN is a crucial yet challenging task. Furthermore, the absence of such algorithms has left many important questions about mixed-state entanglement unexplored.

In this letter, we fill the gap by presenting an efficient QMC algorithm within the *reweight-annealing frame* [75–78]. The named annealing scheme, a specific incremental approach in the algorithm, allows for high precision while maintaining ease of implementation, as it avoids modifications to the entangled regions and boundary condition of imaginary time during simulations. Moreover, the algorithm can naturally generate a continuous RN curve across parameter space and is inherently parallelizable. It enables us to track the variation of RN with respect to a relevant parameter, which is important for understanding many-body entanglement in different phases and at critical points. We demonstrate its capacity in (i) the tripartite 1D antiferromagnet dimerized Heisenberg model (ADHM) at zero temperature, (ii) the bipartite 1D and 2D transverse field Ising models (TFIM) by varying the external field strength at zero temperature, and (iii) the bipartite 2D TFIM by adjusting temperature with weak external fields. Not only the information of the underlying CFTs are achieved, but the roles of entanglement in quantum and thermal phase transitions are revealed in this work.

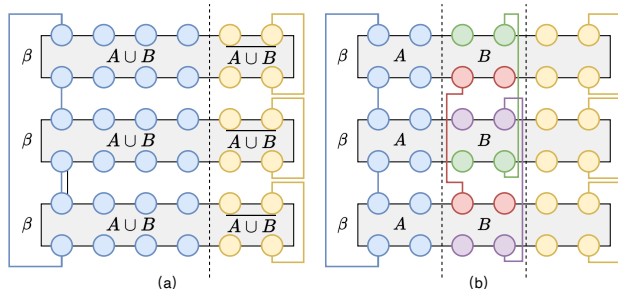


FIG. 1. The horizontal axis represents spatial spins (depicted as circles), while the vertical axis corresponds to imaginary time. Spins of the same color are connected (or glued) along the imaginary time direction by straight lines of the same color. (a) Manifold for Z_3 : The three replicas are sequentially connected along the imaginary time direction for the system $A \cup B$. The environment, denoted by $\overline{A \cup B}$, is traced out by imposing periodic boundary conditions on each replica. (b) manifold for Z_n^{TB} : The connections among three replicas in subsystem A (the blue part) and the environment $\overline{A \cup B}$ (the yellow part) remain identical to that in the left manifold. However, in subsystem B , the connections are not in sequence due to the operation T_B .

Basic idea.— For convenience, we define two generalized partition functions: $Z_n := \text{tr}(\rho^n)$ and $Z_n^{TB} := \text{tr}[(\rho^{TB})^n]$, which correspond to two types of manifolds (illustrated by $n = 3$ in Fig. 1) in the path integral formulation. Thus $R_n = -\ln Z_n^{TB}/Z_n$. Here, we define $\rho := e^{-\beta H}$, which is not normalized in the context of QMC. Typically, Z_n^{TB} ,

Z_n and R_n are functions of some real parameter $\lambda > 0$ (such as temperature or a Hamiltonian parameter). Our starting point is to consider the difference of R_n at two different parameter points λ' and λ'' ($\lambda' < \lambda''$), such that

$$R_n(\lambda'') - R_n(\lambda') = \ln \frac{Z_n^{TB}(\lambda')}{Z_n^{TB}(\lambda'')} - \ln \frac{Z_n(\lambda')}{Z_n(\lambda'')}. \quad (2)$$

The ratio $[Z_n^{TB}(\lambda')/Z_n^{TB}(\lambda'')]$ in Eq. (2) can be further interpreted as a *reweighting operation* [79–81]. If express $Z_n^{TB}(\lambda) = \sum_i W_i(\lambda)$, where $\{W_i(\lambda)\}$ are the weights, then the ratio can be viewed as the average of weight ratios, since $Z_n^{TB}(\lambda')/Z_n^{TB}(\lambda'') = \langle W(\lambda')/W(\lambda'') \rangle_{Z_n^{TB}(\lambda'')}$, where $W(\lambda) \in \{W_i(\lambda)\}$ and the expectation is computed with respect to samples from $Z_n^{TB}(\lambda'')$. The specific form of the estimator $\langle W(\lambda')/W(\lambda'') \rangle_{Z_n^{TB}(\lambda'')}$ depends on the QMC method we use, which transforms the quantum degrees of freedom in $Z_n^{TB}(\lambda')$ to some classical ones. For illustration, we use the stochastic series expansion (SSE) method in this letter [82–85], and the corresponding estimators can be found in the supplemental materials (SM). Similarly, we can apply the same reasoning to $[Z_n(\lambda')/Z_n(\lambda'')]$. It is important to emphasize that the view of reweighting is crucial, as it allows us to estimate the difference $[R_n(\lambda'') - R_n(\lambda')]$ from Eq. (2) by estimating $[Z_n^{TB}(\lambda')/Z_n^{TB}(\lambda'')]$ and $[Z_n(\lambda')/Z_n(\lambda'')]$ in QMC simulations. Additionally, to avoid overflow/underflow issues, we have to store their logarithms in computers.

The procedure described above is sufficient to derive the relative values of $R_n(\lambda)$ at different λ'' when λ' is fixed at λ_0 , called a *reference point*. This allows for the study of various behaviors, such as locating extreme values and singularities of $R_n(\lambda)$. Moreover, if $R_n(\lambda_0)$ is known, we can compute the exact values of $R_n(\lambda)$. Typically, finding such a reference point is straightforward. For example, when $\lambda = \beta \equiv 1/T$, the inverse temperature, we can set $\beta_0 = 0$, which corresponds to a completely disordered system where both classical and quantum correlations are destroyed, giving $R_n(\beta_0) = 0$. In practice, we use a sufficiently small value (e.g. $\beta_0 = 10^{-8}$) in our simulations, and the adequacy of the choice can be verified by considering a smaller one to check the convergence. Similarly, when λ represents the coupling strength of interacting terms in a Hamiltonian related to the entangled boundary, setting $\lambda_0 = 0$ would make the two subsystems completely independent, resulting in $R_n(\lambda_0) = 0$ again. Therefore, depending on our choice of λ , both finite and zero temperature properties of R_n can be explored. For illustrative purpose, we now set $\lambda = \beta$, and other choices of λ can be similarly discussed. By identifying $\lambda_0 \equiv \beta_0 \equiv 0$, Eq. (2) can be reformulated as

$$R_n(\beta) = \ln \frac{Z_n^{TB}(0)}{Z_n^{TB}(\beta)} - \ln \frac{Z_n(0)}{Z_n(\beta)}. \quad (3)$$

Importance sampling and annealing scheme.— Although the ideas of reweighting and reference point are simple, simulations become inefficient if β is far away from β_0

in the parameter space, due to the significant differences between the distributions $Z_n^{TB}(\beta)$ and $Z_n^{TB}(\beta_0)$, requiring an excessive number of samples. To address this, we divide $[\beta_0, \beta]$ into m small subintervals, i.e.

$$\begin{aligned} \ln \frac{Z_n^{TB}(0)}{Z_n^{TB}(\beta)} &= \sum_{k=1}^m \ln \frac{Z_n^{TB}(\beta_{k-1})}{Z_n^{TB}(\beta_k)} \\ \ln \frac{Z_n(0)}{Z_n(\beta)} &= \sum_{k=1}^m \ln \frac{Z_n(\beta_{k-1})}{Z_n(\beta_k)}, \end{aligned} \quad (4)$$

where $\beta_m \equiv \beta$. Then, efficient estimation is ensured when adjacent β_k values are close to satisfy the importance sampling [86]. In addition, the method's effectiveness depends on how $[\beta_0, \beta]$ is divided, as the computational cost also scales with the number of subintervals. Simple approaches, such as equal divisions or geometric progressions with large/small ratios, are inefficient since the required number of subinterval density varies across parameter regions and different system sizes.

To address the problem, we adopt the *annealing scheme*, which requires a polynomial number of subintervals and has demonstrated excellent performance in practical partition function calculations [75]. The core idea is to approximately restrict $[Z_n^{TB}(\beta_{k-1})/Z_n^{TB}(\beta_k)]$ and $[Z_n(\beta_{k-1})/Z_n(\beta_k)]$ to be some constant $\epsilon \lesssim 1$ for all sizes and β_k , to ensure the importance sampling. With some calculations, we find that the total number of subintervals $F(L)$ required scales as $F(L) \approx (\beta - \beta_0)\Lambda n L^d / |\ln \epsilon|$, where d is the system dimension, L is the length of system, and Λ is a constant related to the energy density. Notably, an incorrect choice of Λ just effectively changes the value of ϵ , making ϵ the sole hyperparameter in the algorithm. Similarly, one can discuss when λ is some other parameter in the Hamiltonian, and the division number also scales polynomially with the system size. Further details, including the derivation of $F(L)$ can be found in the SM.

Ground states of tripartite 1D ADHM.- For the first example, we consider a 1D ring of ADHM whose Hamiltonian is $H_{\text{ADHM}} = \sum_{i \in \text{odd}} \mathbf{S}_i \cdot \mathbf{S}_{i+1} + K \sum_{i \in \text{even}} \mathbf{S}_i \cdot \mathbf{S}_{i+1}$. We partition the system into three connected and equally sized regions: subsystems A , B , and the environment $\overline{A \cup B}$, with boundary bonds having a coupling strength of K . When $K = 0$, the three regions A , B , and $\overline{A \cup B}$ are completely independent, thus we take $K_0 = 0$ as the reference point and gradually increase K from K_0 to $K = 1$ in simulations. By tracing out the environment $\overline{A \cup B}$ according to Fig. 1, the entanglement between subsystem A and B is in the context of mixed state. As shown in Fig. 2(a), the entanglement quantified by R_3 increases monotonically when increasing K . This indicates that the entanglement between A and B arises from the Heisenberg interaction at the boundaries. Moreover, at $K = 1$, the model is described by a (1+1)D

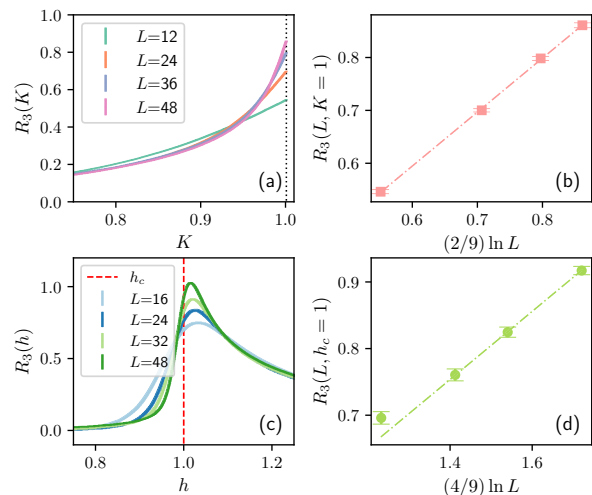


FIG. 2. With $\beta = L$ to extrapolate to the ground state: (a) The variation of $R_3(K)$ with respect to the parameter K for the tripartite (1+1)D DHM ring; (b) The central charge $c = 1.02(2)$ of the underlying CFT for the Heisenberg model is fitted; (c) The variation of $R_3(h)$ with respect to the parameter h for the (1+1)D TFIM under half bipartition; (d) The central charge of the underlying CFT at the critical point is fitted to be $c = 0.51(3)$. Notably, the data of $L = 16$, which exhibits significant finite-size effects and clearly deviates from the trend, is excluded from the fitting.

CFT, and R_n satisfies [42, 43]

$$R_n = \begin{cases} \frac{c}{12} \left(n - \frac{1}{n}\right) \ln \left(\frac{L}{\pi a} \frac{\sin \frac{\pi l_1}{L} \sin \frac{\pi l_2}{L}}{\sin \frac{\pi(l_1+l_2)}{L}} \right) + \mathcal{O}(1), & n \in \text{odd} \\ \frac{c}{6} \left(\frac{n}{2} - \frac{2}{n}\right) \ln \left(\frac{L}{\pi a} \frac{\sin \frac{\pi l_1}{L} \sin \frac{\pi l_2}{L}}{\sin \frac{\pi(l_1+l_2)}{L}} \right) + \mathcal{O}(1), & n \in \text{even} \end{cases} \quad (5)$$

where c is the central charge, a is the lattice constant, L is total length of the ring, and l_1 and l_2 are the lengths of subsystems A and B , respectively. Note that the standard negativity \mathcal{E} can be obtained through taking $n \rightarrow 1$ for even n . For $n = 3$, we therefore have $R_3 \propto (2c/9) \ln L$. As shown in Fig. 2(b), by fitting $R_3(K = 1)$ with the data, we successfully extract $c = 1.02(2)$, which is consistent with the theoretical value 1 [87].

Ground states of bipartite 1D TFIM.- We next consider the TFIM, and the Hamiltonian is given by $H = -\sum_{\langle ij \rangle} Z_i Z_j - h \sum_i X_i$, where $\langle ij \rangle$ denotes the nearest neighbor. For the 1D ring, we consider half bipartition without the environment. By fixing $J = 1$, the quantum critical point (QCP) is at $h_c = 1$, which is also described by a CFT with central charge $c_{\text{Ising}} = 1/2$. We take $h_0 = 0$ to be the reference point, and Fig. 2(c) shows that $R_3(h)$ is maximized at the QCP. When increasing the system length L , it is observed that $R_3(L, h_c)$ diverges. In addition, in the case of half bipartition, R_n

satisfies

$$R_n(h_c) = \begin{cases} \frac{c}{6}(n - \frac{1}{n}) \ln \left(\frac{L}{\pi a} \sin \frac{\pi l}{L} \right) + \mathcal{O}(1), & n \in \text{odd} \\ \frac{c}{3}(\frac{n}{2} - \frac{2}{n}) \ln \left(\frac{L}{\pi a} \sin \frac{\pi l}{L} \right) + \mathcal{O}(1), & n \in \text{even} \end{cases} \quad (6)$$

for a (1+1)D CFT, where l is the length of subsystems A and B . With Eq. (6), the central charge is obtained to be $c = 0.51(3)$, which also accords with the theoretical value. Physically, for both the tripartite 1D ADHM above and this bipartite 1D TFIM, the logarithmic correction of R_n at the CFT points, which is beyond the area law, reflects the existence of long-range entanglement.

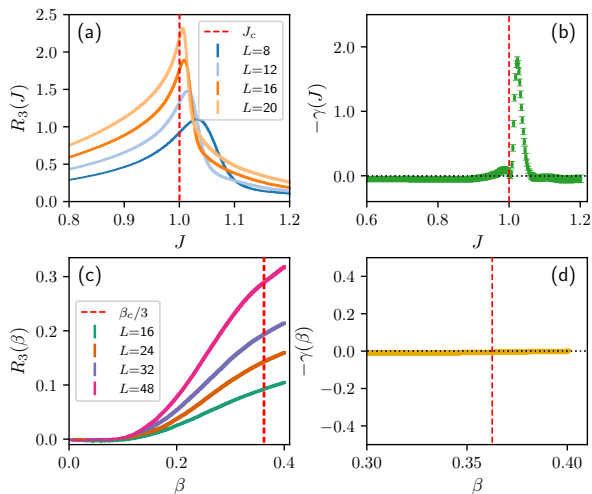


FIG. 3. For the 2D TFIM on the square lattice: (a) fixing $h = 3.04438$, the variation of $R_3(J)$ as a function of J , where $\beta = L$ to extrapolate to the ground state; (b) the area law correction $-\gamma(J)$ of $R_3(J)$ for $J \in [0, 1.2]$, and the inset shows the fitting of the area law at $J = J_c$, where $-\gamma(J_c) = 0.02(5)$; (c) fixing $J = 1$ and $h = 2.75$, the variation of $R_3(\beta)$ as a function of β . (d) the area law correction $-\gamma(\beta)$ of $R_3(\beta)$ for $\beta \in (0, 0.4]$, and the inset shows the fitting of the area law at $\beta = \beta_c/3$, where $-\gamma(\beta_c) = 0.002(7)$;

Ground states and Gibbs states of bipartite 2D TFIM.

We similarly investigated R_3 of the 2D TFIM on a $L \times L$ square lattice with periodic boundary condition, considering the cornerless half-bipartition. The QCP of its ground state occurs at $h/J = 3.04438(2)$ [88]. For convenience, we fix $h = h_c \equiv 3.04438$ and tune J , so that the QCP is positioned at $J_c \approx 1$. To study the ground-state entanglement, we consider R_3 as a function of J and take $J_0 = 0$ as the reference point. Furthermore, when $h/J < 3.04438$, increasing the temperature can induce a thermal phase transition from a ferromagnetic to a paramagnetic phase [89]. Thus we can set a large h to highlight the quantum fluctuations, and study the finite-temperature mixed-state entanglement across a thermal critical point (TCP). We choose $J = 1$ and $h = 2.75$, and the TCP located at $\beta_c = 1/T_c = 1.0874(1)$ [64].

For the ground states, Fig. 3(a) illustrates the behav-

ior of $R_3(J)$ as a function of J for different system sizes. Similar to the 1D TFIM, $R_3(J)$ reaches a maximum and diverges at the QCP, indicating that the QCP exhibits stronger quantum correlations compared to the gapped phases. In the gapped phases, no long-range entanglement is expected, and we should have $R_3 \sim aL - \gamma$ with $\gamma = 0$. Near the critical point, we observe that the area law breaks down, with R_3 for small system sizes exceeding that of larger sizes. However, as the system moves further from the critical point, the area law is restored. If we forcibly fit R_3 to the area law, the constant term γ fluctuates significantly near the critical point, as shown in Fig. 3(b). In other regions, it remains zero within error bars. In principle, R_n can be understood as the difference of free energies between two space-time manifolds with different boundary conditions. Since the only distinction lies at the boundary, it should follow an area law. The deviation from the area law in our numerical data is due to finite-size effects in both space and time, as the gaplessness related to the phase transition requires larger system sizes. Further details on finite-size effects are provided in the SM. Notably, RN inherently removes the contribution of ground state degeneracy due to the denominator in its definition, whereas EE captures it in the correction term as $\gamma = -\ln(N_{\text{deg}})$, where N_{deg} denotes the ground state degeneracy [90]. In this example of ferromagnetic phase, we have $\gamma = 0$.

For the Gibbs states, we take $\beta_0 = 0$ to be the reference point, and Fig. 3(c) shows that $R_3(\beta)$ increases monotonically from the infinite high temperature β_0 to $\beta = 0.4$. Notably, the three replicas effectively scale the inverse temperature by a factor of $1/3$ in partition function Z_3 , and the related critical properties are shifted to $\beta_c/3$ [91]. This has been confirmed in the calculation of the divergence of the first derivative of a , the area-law coefficient of R_3 , in the quantum spherical model and 2D TFIM [64]. As seen in Fig. 3(c), at the critical point $\beta_c/3$, no significant behavior associated with the TCP is observed for R_3 in our calculations. Furthermore, we find that R_3 perfectly obeys the area law and $\gamma \sim 0$ for all the β we computed, as shown in Fig. 3(d). This observation is consistent with the fact that the phase transition is driven by thermal fluctuations, while quantum phase transitions in the 1D TFIM, whose QCP shares the universality class with the TCP, is governed by quantum fluctuations. Consequently, no quantum effects can contribute to the generation of a nonzero and nonlocal term γ in R_3 [58, 59, 69]. Although this conclusion may seem straightforward, it was previously difficult to observe. Moreover, the increase in R_3 when decreasing the temperature reflects an enhancement of quantum properties. However, the quantum correlations remain short range ($\gamma \sim 0$), indicating that the phases beyond or below the TCP are both trivial in terms of quantum correlation.

In addition, we discuss the derivatives of R_n with respect to some parameter λ . Given that $R_n(\lambda) = -\ln Z_n^{TB}(\lambda) + \ln Z_n(\lambda)$, it follows that if the k th-order derivatives of both effective free energy terms are non-

singular at λ , then $d^k R_n(\lambda)/d\lambda^k$ must also remain non-singular. Moreover, since the difference between the two systems associated with Z_n^{TB} and Z_n arises solely from their boundary conditions, their critical points λ_c should remain identical in the thermodynamic limit. Consequently, any singularity in a higher-order derivative of R_n must occur precisely at λ_c .

Summary and discussions.- We have introduced an efficient algorithm for calculating Rényi negativity in quantum Monte Carlo simulations, built on the reweight-annealing framework. This algorithm is easy to implement, has polynomial computational complexity, and is naturally parallelizable. By enabling the calculation of Rényi negativity along a full parameter trajectory in parameter space, our method proves highly versatile. It is not only valuable for investigating entanglement behavior across different phases and near critical points, but also for fitting correction terms in area laws to extract universal quantities such as central charge and topological order in quantum many-body systems. We have validated the

approach in various scenarios, including 1D and 2D systems, ground and Gibbs states, as well as bipartition and tripartition setups. Our results of the Rényi negativity further reveals a detailed understanding of the intrinsic mechanisms governing thermal and quantum critical points in many-body systems.

Acknowledgements.- The authors sincerely thank Tsung-Cheng Lu for kindness and valuable discussions. The authors also thank Fo-Hong Wang, Wei Zhu, Rui-Zhen Huang, and Ying-Jer Kao for their helpful discussions. The work is supported by the Scientific Research Project (No.WU2024B027) and the Start-up Funding of Westlake University. ZW is supported by the China Postdoctoral Science Foundation under Grants No.2024M752898. BBM acknowledge the Natural Science Foundation of Shandong Province, China (Grant No. ZR2024QA194) and NSFC Grant No. 12247101. The authors thank the high-performance computing center of Westlake University and the Beijing PARATERA Tech Co.,Ltd. for providing HPC resources.

-
- [1] Subir Sachdev, “Quantum phase transitions,” *Physics world* **12**, 33 (1999).
- [2] Evgenii Mikhailovich Lifshitz and Lev Petrovich Pitaevskii, *Statistical physics: theory of the condensed state*, Vol. 9 (Elsevier, 2013).
- [3] Luigi Amico, Rosario Fazio, Andreas Osterloh, and Vlatko Vedral, “Entanglement in many-body systems,” *Reviews of modern physics* **80**, 517–576 (2008).
- [4] Nicolas Laflorencie, “Quantum entanglement in condensed matter systems,” *Physics Reports* **646**, 1–59 (2016).
- [5] Bei Zeng, Xie Chen, Duan-Lu Zhou, Xiao-Gang Wen, *et al.*, *Quantum information meets quantum matter* (Springer, 2019).
- [6] A. B. Kallin, E. M. Stoudenmire, P. Fendley, R. R. P. Singh, and R. G. Melko, “Corner contribution to the entanglement entropy of an O(3) quantum critical point in 2 + 1 dimensions,” *J. Stat. Mech.* **2014**, 06009 (2014), arXiv:1401.3504.
- [7] Johannes Helmes and Stefan Wessel, “Entanglement entropy scaling in the bilayer heisenberg spin system,” *Phys. Rev. B* **89**, 245120 (2014).
- [8] Jiarui Zhao, Yan-Cheng Wang, Zheng Yan, Meng Cheng, and Zi Yang Meng, “Scaling of entanglement entropy at deconfined quantum criticality,” *Physical Review Letters* **128**, 010601 (2022).
- [9] Jiarui Zhao, Bin-Bin Chen, Yan-Cheng Wang, Zheng Yan, Meng Cheng, and Zi Yang Meng, “Measuring rényi entanglement entropy with high efficiency and precision in quantum monte carlo simulations,” *npj Quantum Materials* **7**, 69 (2022).
- [10] Max A Metlitski and Tarun Grover, “Entanglement entropy of systems with spontaneously broken continuous symmetry,” arXiv preprint arXiv:1112.5166 (2011).
- [11] Jonathan D’Emidio, “Entanglement entropy from nonequilibrium work,” *Phys. Rev. Lett.* **124**, 110602 (2020).
- [12] Zehui Deng, Lu Liu, Wenan Guo, and HQ Lin, “Improved scaling of the entanglement entropy of quantum antiferromagnetic heisenberg systems,” *Physical Review B* **108**, 125144 (2023).
- [13] Zhe Wang, Zhiyan Wang, Yi-Ming Ding, Bin-Bin Mao, and Zheng Yan, “A quantum monte carlo algorithm to extract large-scale data of entanglement entropy and its derivative in high precision,” (2024), arXiv:2406.05324 [cond-mat.str-el].
- [14] Pasquale Calabrese and Alexandre Lefevre, “Entanglement spectrum in one-dimensional systems,” *Phys. Rev. A* **78**, 032329 (2008).
- [15] Eduardo Fradkin and Joel E. Moore, “Entanglement entropy of 2d conformal quantum critical points: Hearing the shape of a quantum drum,” *Phys. Rev. Lett.* **97**, 050404 (2006).
- [16] H. Casini and M. Huerta, “Universal terms for the entanglement entropy in 2+1 dimensions,” *Nuclear Physics B* **764**, 183–201 (2007).
- [17] Wenjie Ji and Xiao-Gang Wen, “Noninvertible anomalies and mapping-class-group transformation of anomalous partition functions,” *Phys. Rev. Research* **1**, 033054 (2019).
- [18] Qi-Cheng Tang and Wei Zhu, “Critical scaling behaviors of entanglement spectra,” *Chinese Physics Letters* **37**, 010301 (2020).
- [19] Alexei Kitaev and John Preskill, “Topological entanglement entropy,” *Phys. Rev. Lett.* **96**, 110404 (2006).
- [20] Michael Levin and Xiao-Gang Wen, “Detecting topological order in a ground state wave function,” *Phys. Rev. Lett.* **96**, 110405 (2006).
- [21] Sergei V. Isakov, Matthew B. Hastings, and Roger G. Melko, “Topological entanglement entropy of a bose-hubbard spin liquid,” *Nature Physics* **7**, 772 – 775 (2011).
- [22] Zohar Nussinov and Gerardo Ortiz, “Sufficient symmetry conditions for Topological Quantum Order,” *Proc. Nat. Acad. Sci.* **106**, 16944–16949 (2009).
- [23] Zohar Nussinov and Gerardo Ortiz, “A symmetry principle for topological quantum order,” *Annals Phys.* **324**,

- 977–1057 (2009).
- [24] Zheng Yan, Lode Pollet, Jie Lou, Xiaoqun Wang, Yan Chen, and Zi Cai, “Interacting lattice systems with quantum dissipation: A quantum monte carlo study,” *Phys. Rev. B* **97**, 035148 (2018).
- [25] Yichen Huang, “Computing quantum discord is n-complete,” *New Journal of Physics* **16**, 033027 (2014).
- [26] Luigi Amico, Rosario Fazio, Andreas Osterloh, and Vlatko Vedral, “Entanglement in many-body systems,” *Rev. Mod. Phys.* **80**, 517–576 (2008).
- [27] Ryszard Horodecki, Paweł Horodecki, Michał Horodecki, and Karol Horodecki, “Quantum entanglement,” *Rev. Mod. Phys.* **81**, 865–942 (2009).
- [28] Jens Eisert and Martin B Plenio, “A comparison of entanglement measures,” *Journal of Modern Optics* **46**, 145–154 (1999).
- [29] G. Vidal and R. F. Werner, “Computable measure of entanglement,” *Phys. Rev. A* **65**, 032314 (2002).
- [30] M. B. Plenio, “Logarithmic negativity: A full entanglement monotone that is not convex,” *Phys. Rev. Lett.* **95**, 090503 (2005).
- [31] K. Audenaert, J. Eisert, M. B. Plenio, and R. F. Werner, “Entanglement properties of the harmonic chain,” *Phys. Rev. A* **66**, 042327 (2002).
- [32] Viktor Eisler and Zoltán Zimborás, “On the partial transpose of fermionic gaussian states,” *New Journal of Physics* **17**, 053048 (2015).
- [33] Cristiano De Nobili, Andrea Coser, and Erik Tonni, “Entanglement negativity in a two dimensional harmonic lattice: area law and corner contributions,” *Journal of Statistical Mechanics: Theory and Experiment* **2016**, 083102 (2016).
- [34] Davide Bianchini and Olalla A. Castro-Alvaredo, “Branch point twist field correlators in the massive free boson theory,” *Nuclear Physics B* **913**, 879–911 (2016).
- [35] Viktor Eisler and Zoltán Zimborás, “Entanglement negativity in two-dimensional free lattice models,” *Phys. Rev. B* **93**, 115148 (2016).
- [36] Hassan Shapourian, Ken Shiozaki, and Shinsei Ryu, “Partial time-reversal transformation and entanglement negativity in fermionic systems,” *Phys. Rev. B* **95**, 165101 (2017).
- [37] Hassan Shapourian and Shinsei Ryu, “Finite-temperature entanglement negativity of free fermions,” *Journal of Statistical Mechanics: Theory and Experiment* **2019**, 043106 (2019).
- [38] Nicholas E. Sherman, Trithap Devakul, Matthew B. Hastings, and Rajiv R. P. Singh, “Nonzero-temperature entanglement negativity of quantum spin models: Area law, linked cluster expansions, and sudden death,” *Phys. Rev. E* **93**, 022128 (2016).
- [39] Asher Peres, “Separability criterion for density matrices,” *Physical Review Letters* **77**, 1413 (1996).
- [40] Paweł Horodecki, “Separability criterion and inseparable mixed states with positive partial transposition,” *Physics Letters A* **232**, 333–339 (1997).
- [41] R. Simon, “Peres-horodecki separability criterion for continuous variable systems,” *Phys. Rev. Lett.* **84**, 2726–2729 (2000).
- [42] Pasquale Calabrese, John Cardy, and Erik Tonni, “Entanglement negativity in quantum field theory,” *Physical review letters* **109**, 130502 (2012).
- [43] Pasquale Calabrese, John Cardy, and Erik Tonni, “Entanglement negativity in extended systems: a field theoretical approach,” *Journal of Statistical Mechanics: Theory and Experiment* **2013**, P02008 (2013).
- [44] Pasquale Calabrese, Luca Tagliacozzo, and Erik Tonni, “Entanglement negativity in the critical ising chain,” *Journal of Statistical Mechanics: Theory and Experiment* **2013**, P05002 (2013).
- [45] Manuela Kulaxizi, Andrei Parnachev, and Giuseppe Policastro, “Conformal blocks and negativity at large central charge,” *Journal of High Energy Physics* **2014**, 1–25 (2014).
- [46] Pasquale Calabrese, John Cardy, and Erik Tonni, “Finite temperature entanglement negativity in conformal field theory,” *Journal of Physics A: Mathematical and Theoretical* **48**, 015006 (2014).
- [47] Cristiano De Nobili, Andrea Coser, and Erik Tonni, “Entanglement entropy and negativity of disjoint intervals in cft: Some numerical extrapolations,” *Journal of Statistical Mechanics: Theory and Experiment* **2015**, P06021 (2015).
- [48] Hannu Wichterich, Javier Molina-Vilaplana, and Sougato Bose, “Scaling of entanglement between separated blocks in spin chains at criticality,” *Physical Review A—Atomic, Molecular, and Optical Physics* **80**, 010304 (2009).
- [49] Paola Ruggiero, Vincenzo Alba, and Pasquale Calabrese, “Entanglement negativity in random spin chains,” *Physical Review B* **94**, 035152 (2016).
- [50] Younes Javanmard, Daniele Trapin, Soumya Bera, Jens H Bardarson, and Markus Heyl, “Sharp entanglement thresholds in the logarithmic negativity of disjoint blocks in the transverse-field ising chain,” *New Journal of Physics* **20**, 083032 (2018).
- [51] Yirum Arthur Lee and Guifre Vidal, “Entanglement negativity and topological order,” *Physical Review A—Atomic, Molecular, and Optical Physics* **88**, 042318 (2013).
- [52] Claudio Castelnovo, “Negativity and topological order in the toric code,” *Physical Review A—Atomic, Molecular, and Optical Physics* **88**, 042319 (2013).
- [53] Xueda Wen, Po-Yao Chang, and Shinsei Ryu, “Topological entanglement negativity in chern-simons theories,” *Journal of High Energy Physics* **2016**, 1–30 (2016).
- [54] Xueda Wen, Shunji Matsuura, and Shinsei Ryu, “Edge theory approach to topological entanglement entropy, mutual information, and entanglement negativity in chern-simons theories,” *Physical Review B* **93**, 245140 (2016).
- [55] Oliver Hart and Claudio Castelnovo, “Entanglement negativity and sudden death in the toric code at finite temperature,” *Physical Review B* **97**, 144410 (2018).
- [56] Tsung-Cheng Lu and Tarun Grover, “Structure of quantum entanglement at a finite temperature critical point,” *Physical Review Research* **2**, 043345 (2020).
- [57] Nicholas E Sherman, Trithap Devakul, Matthew B Hastings, and Rajiv RP Singh, “Nonzero-temperature entanglement negativity of quantum spin models: Area law, linked cluster expansions, and sudden death,” *Physical Review E* **93**, 022128 (2016).
- [58] Tsung-Cheng Lu, Timothy H. Hsieh, and Tarun Grover, “Detecting topological order at finite temperature using entanglement negativity,” *Phys. Rev. Lett.* **125**, 116801 (2020).
- [59] Tsung-Cheng Lu, “Disentangling transitions in topological order induced by boundary decoherence,” (2024),

- arXiv:2404.06514.
- [60] Andreas Elben, Richard Kueng, Hsin-Yuan (Robert) Huang, Rick van Bijnen, Christian Kokail, Marcello Dalmonte, Pasquale Calabrese, Barbara Kraus, John Preskill, Peter Zoller, and Benoît Vermersch, “Mixed-state entanglement from local randomized measurements,” *Phys. Rev. Lett.* **125**, 200501 (2020).
- [61] Chia-Min Chung, Vincenzo Alba, Lars Bonnes, Pochung Chen, and Andreas M. Läuchli, “Entanglement negativity via the replica trick: A quantum monte carlo approach,” *Phys. Rev. B* **90**, 064401 (2014).
- [62] Vincenzo Alba, “Entanglement negativity and conformal field theory: a monte carlo study,” *Journal of Statistical Mechanics: Theory and Experiment* **2013**, P05013 (2013).
- [63] Antoine Neven, Jose Carrasco, Vittorio Vitale, Christian Kokail, Andreas Elben, Marcello Dalmonte, Pasquale Calabrese, Peter Zoller, Benoît Vermersch, Richard Kueng, and Barbara Kraus, “Symmetry-resolved entanglement detection using partial transpose moments,” *npj Quantum Information* **7**, 152 (2021).
- [64] Kai-Hsin Wu, Tsung-Cheng Lu, Chia-Min Chung, Ying-Jer Kao, and Tarun Grover, “Entanglement renyi negativity across a finite temperature transition: A monte carlo study,” *Phys. Rev. Lett.* **125**, 140603 (2020).
- [65] Elisabeth Wybo, Michael Knap, and Frank Pollmann, “Entanglement dynamics of a many-body localized system coupled to a bath,” *Phys. Rev. B* **102**, 064304 (2020).
- [66] Fo-Hong Wang and Xiao Yan Xu, “Entanglement renyi negativity of interacting fermions from quantum monte carlo simulations,” (2023), arXiv:2312.14155.
- [67] Ruihua Fan, Yimu Bao, Ehud Altman, and Ashvin Vishwanath, “Diagnostics of mixed-state topological order and breakdown of quantum memory,” *PRX Quantum* **5**, 020343 (2024).
- [68] Tsung-Cheng Lu and Tarun Grover, “Singularity in entanglement negativity across finite-temperature phase transitions,” *Phys. Rev. B* **99**, 075157 (2019).
- [69] Tsung-Cheng Lu and Tarun Grover, “Structure of quantum entanglement at a finite temperature critical point,” *Phys. Rev. Res.* **2**, 043345 (2020).
- [70] Jeongmin Shim, H.-S. Sim, and Seung-Sup B. Lee, “Numerical renormalization group method for entanglement negativity at finite temperature,” *Phys. Rev. B* **97**, 155123 (2018).
- [71] Chia-Min Chung, Lars Bonnes, Pochung Chen, and Andreas M. Läuchli, “Entanglement spectroscopy using quantum monte carlo,” *Phys. Rev. B* **89**, 195147 (2014).
- [72] Kai-Hsin Wu, Tsung-Cheng Lu, Chia-Min Chung, Ying-Jer Kao, and Tarun Grover, “Entanglement renyi negativity across a finite temperature transition: a monte carlo study,” *Physical Review Letters* **125**, 140603 (2020).
- [73] Matthew B. Hastings, Iván González, Ann B. Kallin, and Roger G. Melko, “Measuring renyi entanglement entropy in quantum monte carlo simulations,” *Phys. Rev. Lett.* **104**, 157201 (2010).
- [74] Stephan Humeniuk and Tommaso Roscilde, “Quantum monte carlo calculation of entanglement renyi entropies for generic quantum systems,” *Phys. Rev. B* **86**, 235116 (2012).
- [75] Yi-Ming Ding, Jun-Song Sun, Nvsen Ma, Gaopei Pan, Chen Cheng, and Zheng Yan, “Reweight-annealing method for evaluating the partition function via quantum monte carlo calculations,” *Phys. Rev. B* **110**, 165152 (2024).
- [76] Zhe Wang, Zhiyan Wang, Yi-Ming Ding, Bin-Bin Mao, and Zheng Yan, “Bipartite reweight-annealing algorithm to extract large-scale data of entanglement entropy and its derivative in high precision,” (2024), arXiv:2406.05324.
- [77] Weilun Jiang, Gaopei Pan, Zhe Wang, Bin-Bin Mao, Heng Shen, and Zheng Yan, “High-efficiency quantum monte carlo algorithm for extracting entanglement entropy in interacting fermion systems,” (2024), arXiv:2409.20009.
- [78] Yi-Ming Ding, Zhe Wang, and Zheng Yan, “Evaluating many-body stabilizer renyi entropy by sampling reduced pauli strings: singularities, volume law, and non-local magic,” (2025), arXiv:2501.12146.
- [79] Alan M. Ferrenberg and Robert H. Swendsen, “New monte carlo technique for studying phase transitions,” *Phys. Rev. Lett.* **61**, 2635–2638 (1988).
- [80] Alan M. Ferrenberg and Robert H. Swendsen, “Optimized monte carlo data analysis,” *Phys. Rev. Lett.* **63**, 1195–1198 (1989).
- [81] Matthias Troyer, Fabien Alet, and Stefan Wessel, “Histogram methods for quantum systems: from reweighting to wang-landau sampling,” *Brazilian Journal of Physics* **34** (2004), 10.1590/s0103-97332004000300008.
- [82] Anders W. Sandvik, “Stochastic method for analytic continuation of quantum monte carlo data,” *Phys. Rev. B* **57**, 10287–10290 (1998).
- [83] Anders W Sandvik, “Stochastic series expansion method for quantum ising models with arbitrary interactions,” *Physical Review E* **68**, 056701 (2003).
- [84] Zheng Yan, Yongzheng Wu, Chenrong Liu, Olav F Syljuåsen, Jie Lou, and Yan Chen, “Sweeping cluster algorithm for quantum spin systems with strong geometric restrictions,” *Physical Review B* **99**, 165135 (2019).
- [85] Zheng Yan, “Global scheme of sweeping cluster algorithm to sample among topological sectors,” *Phys. Rev. B* **105**, 184432 (2022).
- [86] Radford M Neal, “Annealed importance sampling,” *Statistics and computing* **11**, 125–139 (2001).
- [87] H. W. J. Blöte, John L. Cardy, and M. P. Nightingale, “Conformal invariance, the central charge, and universal finite-size amplitudes at criticality,” *Phys. Rev. Lett.* **56**, 742–745 (1986).
- [88] Henk W. J. Blöte and Youjin Deng, “Cluster monte carlo simulation of the transverse ising model,” *Phys. Rev. E* **66**, 066110 (2002).
- [89] S. Hesselmann and S. Wessel, “Thermal ising transitions in the vicinity of two-dimensional quantum critical points,” *Phys. Rev. B* **93**, 155157 (2016).
- [90] Jean-Marie Stéphan, Shunsuke Furukawa, Grégoire Misguich, and Vincent Pasquier, “Shannon and entanglement entropies of one- and two-dimensional critical wave functions,” *Phys. Rev. B* **80**, 184421 (2009).
- [91] The term $\text{tr}(\rho^3) \propto \text{tr}(e^{-3\beta H})$ will lead a singularity at $\beta_c/3$.
- [92] Zheng Zhou, Changle Liu, Zheng Yan, Yan Chen, and Xue-Feng Zhang, “Quantum dynamics of topological strings in a frustrated ising antiferromagnet,” *npj Quantum Materials* **7**, 60 (2022).
- [93] Zheng Zhou, Changle Liu, Dong-Xu Liu, Zheng Yan, Yan Chen, and Xue-Feng Zhang, “Quantum tricriticality of incommensurate phase induced by quantum strings

in frustrated Ising magnetism,” *SciPost Phys.* **14**, 037 (2023).

[94] Zheng Yan, Zheng Zhou, Yan-Hua Zhou, Yan-Cheng Wang, Xingze Qiu, Zi Yang Meng, and Xue-Feng

Zhang, “Quantum optimization within lattice gauge theory model on a quantum simulator,” *npj Quantum Information* **9**, 89 (2023).

I. ESTIMATORS IN REWEIGHTING OPERATIONS

We focus the stochastic series expansion (SSE) method [82–85], and other quantum Monte Carlo (QMC) methods can be similarly discussed in principle. If $\lambda = \beta$, the estimators for $[Z_n^{T_B}(\beta_{k-1})/Z_n^{T_B}(\beta_k)]$ and $[Z_n(\beta_{k-1})/Z_n(\beta_k)]$ are universal as long as the model is sign-problem free. For a given Hamiltonian H and $\rho = e^{-\beta H}$, we have

$$\begin{aligned} Z_n^{T_B}(\beta_{k-1}) &= \text{tr}(\{\rho^{T_B}\}^n) \\ &= \text{tr}\left(\left\{\left[\sum_{s=0}^{\infty} \frac{\beta_{k-1}^s}{s!} (-H)^s\right]^{T_B}\right\}^n\right) \\ &= \text{tr}\left(\left\{\left[\sum_{s=0}^{\infty} \left(\frac{\beta_{k-1}}{\beta_k}\right)^s \frac{\beta_k^s}{s!} (-H)^s\right]^{T_B}\right\}^n\right), \end{aligned} \quad (1)$$

where s is the order of Taylor expansion, i.e., the total number of non-identity operators of the SSE configuration. Therefore, we have

$$\frac{Z_n^{T_B}(\beta_{k-1})}{Z_n^{T_B}(\beta_k)} = \left\langle \left(\frac{\beta_{k-1}}{\beta_k}\right)^s \right\rangle_{Z_n^{T_B}(\beta_k)}, \quad (2)$$

where $\langle \dots \rangle_{Z_n^{T_B}(\beta_k)}$ means that the sampling is performed on $Z_n^{T_B}(\beta_k)$. Similarly,

$$\frac{Z_n(\beta_{k-1})}{Z_n(\beta_k)} = \left\langle \left(\frac{\beta_{k-1}}{\beta_k}\right)^s \right\rangle_{Z_n(\beta_k)} \quad (3)$$

If λ is a non-temperature parameter, the estimators typically depend on the model.

For example, if $\lambda = h$ in the Hamiltonian

$$H = - \sum_{\langle ij \rangle} Z_i Z_j - h \sum_i X_i \quad (4)$$

of the transverse field Ising model (TFIM), we have

$$\frac{Z_n^{T_B}(h_{k-1})}{Z_n^{T_B}(h_k)} = \left\langle \left(\frac{h_{k-1}}{h_k}\right)^{s_h} \right\rangle_{Z_n^{T_B}(h_k)} \quad (5)$$

$$\frac{Z_n(h_{k-1})}{Z_n(h_k)} = \left\langle \left(\frac{h_{k-1}}{h_k}\right)^{s_h} \right\rangle_{Z_n(h_k)} \quad (6)$$

where s_h is the number of operators related to the transverse field h only in the series expansions no matter in the manifold $Z_n^{T_B}(h_k)$ or $Z_n(h_k)$. The details of the SSE algorithm for TFIM can be found in Ref. [83, 92–94].

II. ANNEALING SCHEME ($\lambda = \beta$)

The target of the annealing scheme is to provide an economic way to divide $[\beta_0, \beta]$ into m subintervals $\{[\beta_{k-1}, \beta_k]\}$ to ensure the importance sampling, such that we can compute $[Z_n^{T_B}(\beta_0)/Z_n^{T_B}(\beta)]$ and $[Z_n(\beta_0)/Z_n(\beta)]$ via

$$\begin{aligned} \frac{Z_n^{T_B}(0)}{Z_n^{T_B}(\beta)} &= \prod_{k=1}^m \frac{Z_n^{T_B}(\beta_{k-1})}{Z_n^{T_B}(\beta_k)} \\ \frac{Z_n(0)}{Z_n(\beta)} &= \prod_{k=1}^m \frac{Z_n(\beta_{k-1})}{Z_n(\beta_k)} \end{aligned} \quad (7)$$

Remember that we have choose the reference point $\beta_0 \equiv 0$. We mainly focus on $\lambda = \beta$ in this material, and it is similar to discuss other choices of λ . The slight difference will be introduced in the end of the next section.

For a vanilla partition function $Z(\beta) = \text{tr}(e^{-\beta H})$ of some quantum spin model, each classical configuration sampled in SSE simulations is composite of both the states of spins and operators, thus the number of non-identity operators s_{vn} is exactly some observable in this language, which has the relation $E(\beta) = -\langle s_{\text{vn}} \rangle_{Z(\beta)} / \beta$ with the energy $E(\beta)$. In other words, $\langle s_{\text{vn}} \rangle_{Z(\beta)} \sim \beta |E(\beta)|$.

Suppose \bar{s}_{tot} and s_{tot} are the corresponding numbers of non-identity operators of $Z_n^{TB}(\beta)$ and $Z_n(\beta)$. Since $Z_n(\beta) = Z(n\beta)$, we directly obtain $\langle s_{\text{tot}} \rangle_{Z_n(\beta)} = \langle s_{\text{vn}} \rangle_{Z(n\beta)} \sim n\beta |E(\beta)|$. Next, consider \bar{s}_{tot} . In fact, the difference between $\langle \bar{s}_{\text{tot}} \rangle_{Z_n^{TB}(\beta')}$ and $\langle s_{\text{tot}} \rangle_{Z_n(\beta')}$, where $\beta' \in [\beta_0, \beta]$, reflects the existence of entanglement because

$$\begin{aligned} R_n(\beta) &= \ln \frac{Z_n^{TB}(0)}{Z_n^{TB}(\beta)} - \ln \frac{Z_n(0)}{Z_n(\beta)} \\ &= - \int_0^\beta d\beta' \left[\frac{d \ln Z_n^{TB}(\beta')}{d\beta'} - \frac{d \ln Z_n(\beta')}{d\beta'} \right] \\ &= - \int_0^\beta d\beta' \left[\frac{1}{Z_n^{TB}(\beta')} \frac{dZ_n^{TB}(\beta')}{d\beta'} - \frac{1}{Z_n(\beta')} \frac{dZ_n(\beta')}{d\beta'} \right] \\ &= - \int_0^\beta d\beta' \frac{1}{\beta'} \left[\langle \bar{s}_{\text{tot}} \rangle_{Z_n^{TB}(\beta')} - \langle s_{\text{tot}} \rangle_{Z_n(\beta')} \right] \end{aligned} \quad (8)$$

Since the amount of entanglement is an extensive quantity, therefore we should have $\bar{s}_{\text{tot}} \sim n\beta |E(\beta)|$ satisfies as well. With these knowledge, we can now introduce the annealing scheme. We take $[Z_n^{TB}(\beta_{k-1})/Z_n^{TB}(\beta_k)]$ for illustrations, and it is similar to discuss $[Z_n(\beta_{k-1})/Z_n(\beta_k)]$. For brevity, from now, we drop the subscript of $\langle \dots \rangle$, which should be the corresponding $Z_n^{TB}(\beta_k)$, and write $\bar{s}_{\text{tot}} \equiv s$.

We first require $[Z_n^{TB}(\beta_{k-1})/Z_n^{TB}(\beta_k)] = \epsilon < 1$ for all k , where ϵ is some constant close to 1 to ensure the importance sampling when estimating $[Z_n^{TB}(\beta_{k-1})/Z_n^{TB}(\beta_k)]$ with $\langle (\beta_{k-1}/\beta_k)^s \rangle$ at β_k . If $\epsilon = 1$, the two distributions must be exactly the same and this is some trivial reweighting operation. As we mentioned above, s is some observable, therefore we can achieve some estimation s^* for it from simulations (same as we measure the energy) at β_k . Hence, we can bring such an s^* into

$$\epsilon = \left\langle \left(\frac{\beta_{k-1}}{\beta_k} \right)^s \right\rangle \approx \left(\frac{\beta_{k-1}}{\beta_k} \right)^{s^*}. \quad (9)$$

Eq. (9) enables us to determine the position of β_{k-1} only with β_k since

$$\beta_{k-1} = \epsilon^{1/s^*} \beta_k \quad (10)$$

Therefore, if we start from β_m , using Eq. (9), we can determine the rest of $\beta_{m-1}, \dots, \beta_1$, and the procedure stops when we encounter some β_j such that $\beta_{j-1} < \beta_0$. Each determination of β_{k-1} relays on some simulations on β_k , and in this sense, the inverse temperature gradually goes from β_m to β_0 . This is akin to a standard quantum annealing or thermal annealing process where we tune some parameter, so we call this way of dividing $[\beta_0, \beta]$ an annealing scheme.

To enable parallelizations, we can manually set the value of s^* rather than estimating it from simulations. As energy $E \sim L^d$, where L is the system length and d is the dimension, we can set $s^* \simeq \Lambda_k n \beta_k L^d$, where Λ_k is another constant factor related to the energy density. Then, Eq. (10) reduces to

$$\beta_{k-1} = \epsilon^{1/(\Lambda_k n \beta_k L^d)} \beta_k \quad (11)$$

If we manually set the value of Λ_k with some incorrect and uniform Λ , this would effectively change the true value of $[Z_n^{TB}(\beta_{k-1})/Z_n^{TB}(\beta_k)]$ from ϵ , what we set at the beginning, to some other ϵ_k . Therefore the dependence on k can be absorbed into the base, i.e.

$$\beta_{k-1} = \epsilon_k^{1/(\Lambda n \beta_k L^d)} \beta_k \quad (12)$$

If one preknows the variation of $\Lambda_k(\beta)$ or ϵ_k as a function of β , everything would be basically same with that in Eq. (10), but this is not a general case. On another hand, if we further simplify Eq. (12) by setting $\epsilon_k \equiv \epsilon$ for all k , this operation would just make the value of $[Z_n^{TB}(\beta_{k-1})/Z_n^{TB}(\beta_k)]$ achieved in simulations varies with different k , but usually at the same order of magnitude if no critical point lies within $[\beta_0, \beta]$. Such a critical point may change the value of Λ_k sharply near that point. However, our method is not for locating the critical point, which can be

obtained by considering some order parameter or dimensionless quantity such as the Binder cumulant. Therefore, we can assume that we know the position of the critical point, and on the two sides of that point, we can adopt different ϵ to avoid the problem.

To sum up, by manually setting some Λ , we only have one hyperparameter ϵ to determine. Smaller ϵ we choose, more Monte Carlo samples we need to obtain a given precision. However, if ϵ is too large, the number of divisions m may be huge, making the total computational resources unaffordable. This means we need some tradeoff on choosing ϵ . Actually, this is not difficult. By doing some trials on small systems, we can obtain some appropriate ϵ and apply it on larger systems. With this scheme, we can calculate all values of β_k at the beginning without any simulations, therefore different estimations of $[Z_n^{T_B}(\beta_{k-1})/Z_n^{T_B}(\beta_k)]$ can be parallelized on computers, which are further used to estimate $\ln[Z_n^{T_B}(\beta_{k-1})/Z_n^{T_B}(\beta_k)]$ and $R_n(\beta)$.

III. COMPUTATIONAL COMPLEXITY OF THE ANNEALING SCHEME

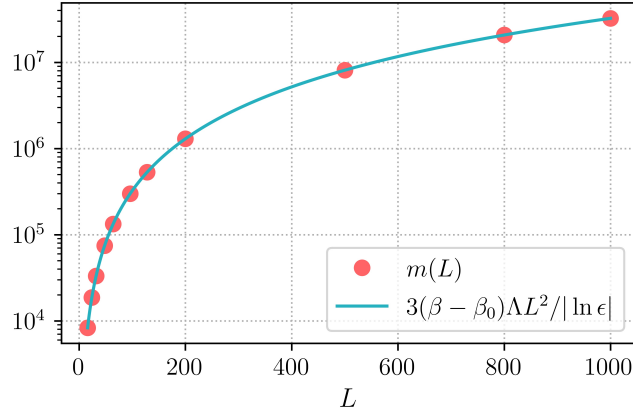


FIG. 1. The number of subintervals $m(L)$ with different L (marked in red circles) calculated with the annealing scheme we introduced. It is perfectly in accordance with the function $F(L) := \Lambda n(\beta - \beta_0)L^d / |\ln \epsilon|$, where $n = 3$ for the third order of Rényi negativity and $d = 2$ for the 2D TFIM model. For example, for $L = 48$ (the largest size we simulated), we have $m(48) = 74813$ and $F(48) = 74804.686$.

In this section, we prove that the annealing scheme makes our algorithm have polynomial computational complexity.

For each $\langle (\beta_{k-1}/\beta_k)^s \rangle \approx \epsilon$ close to 1 to ensure the importance sampling, the number of samples required to efficiently estimate it should not increase exponentially with the system size, provided the relative error does not diverge exponentially. Denote $O \equiv (\beta_{k-1}/\beta_k)^s$, then

$$\frac{\Delta O}{\langle O \rangle} = \frac{\sqrt{\langle O^2 \rangle - \langle O \rangle^2}}{\langle O \rangle \sqrt{N}} = \frac{\sqrt{\langle O^2 \rangle / \langle O \rangle^2 - 1}}{\sqrt{N}} = \frac{\sqrt{\langle O^2 \rangle / \epsilon^2 - 1}}{\sqrt{N}} \quad (13)$$

where N is the number of samples. Remember that $O \in (0, 1]$ for any possible classical configuration in the language of QMC, then $\langle O^2 \rangle \leq \langle O \rangle = \epsilon$, with which we finally obtain

$$\frac{\Delta O}{\langle O \rangle} \leq \frac{\sqrt{1/\epsilon - 1}}{\sqrt{N}} \quad (14)$$

which is indeed finite to any size and temperature. Therefore, as long as the annealing scheme above generates polynomial number of subintervals, the total computational complexity would be finally polynomial.

For large L , we have

$$\beta_{k-1} = \epsilon^{1/(\Lambda n \beta_k L^d)} \beta_k \approx \left(1 + \frac{\ln \epsilon}{\Lambda n \beta_k L^d} \right) \beta_k \quad (15)$$

which means

$$\beta_k - \beta_{k-1} \approx -\frac{\ln \epsilon}{\Lambda n L^d} \beta_k \quad (16)$$

thus the total number of subintervals $m = m(L)$ is around $F(L) = (\beta - \beta_0)\Lambda n L^d / |\ln \epsilon|$, which is indeed polynomial. Here we have ignored the case when β_k is small in Eq. (15). This actually contributes little to the value of $m(L)$ because when $\beta_k \rightarrow 0$, $\epsilon^{1/(\Lambda n \beta_k L^d)} \rightarrow 0$ (remember that $\epsilon < 1$), making the distribution of β_k much more sparser than that of the region where $\beta_k \gg 0$.

In practical simulations on computers, we cannot really take $\beta_0 = 0$, so we set a sufficiently small number such as $\beta_0 = 10^{-8}$ used in our simulations. The adequacy of the choice of β_0 can be checked by considering a smaller one to see whether the result is convergent. For references, in our simulations of the 2D TFIM model, we take $\Lambda = 25h$, $\epsilon = 0.1$ and 50 bins for each $\langle (\beta_{k-1}/\beta_k)^s \rangle$ with 10^4 Monte Carlo steps in each bin. For $\beta = 0.362466667 \approx \beta_c/3$ and $\beta_0 = 10^{-8}$, we calculate the number of subintervals $m(L)$ given by the annealing scheme, which is consistent with our estimation $F(L) = (\beta - \beta_0)\Lambda n L^d / |\ln \epsilon|$, shown in Fig. (1).

Similar discussions can be applied to the case when λ is a coupling strength in the Hamiltonian, and a modification is just replacing β_k with $\lambda\beta_k$ to estimate $\bar{s}_{\lambda, \text{tot}}$ and $s_{\lambda, \text{tot}}$. We find this hypothetical linear relation actually works well practically and has similar performance as above.

IV. FINITE-SIZE EFFECT IN SIMULATING RN

We first revisit the definition of Rényi negativity. In our earlier introduction of the algorithm, we considered an unnormalized density matrix $\rho = e^{-\beta H}$. Here we consider $\rho := e^{-\beta H}/Z$ to be normalized for the convenience of discussions, and the Rényi negativity can be expressed as

$$R_3 := -\ln \frac{\text{tr}[(\rho^{T_B})^3]}{\text{tr}(\rho^3)} = -\ln\{\text{tr}[(\rho^{T_B})^3]\} + \ln\{\text{tr}(\rho^3)\} \quad (17)$$

For a system in a pure state, i.e. $\text{tr}(\rho^n) = 1$, the second term in Eq. (17) vanishes, simplifying the expression to

$$R_3 = -\ln\{\text{tr}[(\rho^{T_B})^3]\} = -\ln\{\text{tr}(\rho_A)^3\} \quad (18)$$

as [43]

$$\text{tr}[(\rho^{T_B})^n] = \begin{cases} \text{tr}(\rho_A)^n & n \in \text{odd} \\ [\text{tr}(\rho_A^{n/2})]^2 & n \in \text{even} \end{cases} \quad (19)$$

where $\rho_A = \text{tr}_B(\rho)$ is the reduced density matrix of the subsystem A .

The entanglement Rényi entropy is defined as

$$S_n(\rho_A) = \frac{1}{1-n} \ln[\text{tr}(\rho_A^n)] \quad (20)$$

which implies that $R_3 = 2S_3$ when ρ corresponds to a pure state. In the context of Monte Carlo simulations, the ground state is achieved by taking the limit $\beta \rightarrow \infty$ for $\rho = e^{-\beta H}/Z$ to filter out the excited states. If the system has a two-fold degeneracy in its ground state (e.g., as in the classical Ising model), we have

$$\begin{aligned} \lim_{\beta \rightarrow \infty} e^{-\beta H} &= \lim_{\beta \rightarrow \infty} \sum_i e^{-\beta E_i} |\psi_i\rangle \langle \psi_i| \\ &= \lim_{\beta \rightarrow \infty} e^{-\beta E_0} \left[|\psi_0\rangle \langle \psi_0| + |\psi'_0\rangle \langle \psi'_0| + \sum_{i \neq 0} e^{-\beta(E_i - E_0)} |\psi_i\rangle \langle \psi_i| \right] \\ &= \lim_{\beta \rightarrow \infty} e^{-\beta E_0} \left[|\psi_0\rangle \langle \psi_0| + |\psi'_0\rangle \langle \psi'_0| \right] \end{aligned} \quad (21)$$

where $\{|\psi_i\rangle\}$ are the eigenstates of the Hamiltonian with $|\psi_0\rangle$ and $|\psi'_0\rangle$ to be the two degenerate ground states. This means that the ground state ρ in QMC is basically a mixed state when the system has some degeneracy.

In QMC simulations, the ground state of a Hamiltonian is typically achieved by taking $\beta \propto L^z$, where z is the dynamical critical exponent at the critical point. This approach ensures extrapolation to the true ground state in the thermodynamic limit ($L \rightarrow \infty$). For all the models we consider in this work, we have $z = 1$, and we set $\beta = L$ to filter out the high-energy states in our work. For finite systems, the energy gap between the asymptotically degenerate ground states vanishes exponentially with system size, and the choice of $\beta = L$ is also sufficient. However, the critical point effectively becomes an extreme (asymptotically gapless) point, which shifts with increasing system size. As a

result, fixing $\beta = L$ or any other linear function of L may lead to a breakdown of the area law near these extreme points, as different system sizes respond differently to gaplessness at the same parameter point.

In closing, we discuss the difference between R_3 and $2S_3$ in quantifying a degenerate ground state. For illustrations, consider a simple example of 1D TFIM with $L = 8$ and $h \equiv 1$. In this finite system, the true ground state remains a pure state as the two-fold degeneracy occurs at the thermodynamic limit, thus the relation $R_3(J, \beta = \infty) = S_3(J, \beta = \infty)$ holds rigorously for all values of J , as shown in Fig. 2. In order to effectively filter out all high-energy states using the projector $e^{-\beta H}$ to achieve a pure state, β must be large enough to distinguish the two lowest energy levels. From Fig. 2, we observe that as β is increased from 16 to 64, the behavior of $R_3(J < 1, \beta)$ remains nearly unchanged, while the behavior of $R_3(J > 1, \beta)$ continues to approach $R_3(J, \beta = \infty)$. Actually, this requirement is for computing S_3 , which is only an entanglement monotone for pure states. For R_3 , there is no need to thoroughly distinguish the two asymptotically degenerate states as we will do the extrapolation with finite systems. In the thermodynamic limit, the emergence of the two-fold degeneracy leads to $\text{tr}(\rho^3) = 1/4$, or equivalently, $\ln[\text{tr}(\rho^3)] = -2 \ln 2 \approx -1.386$. This precisely cancels the area-law correction associated with degeneracy in the entanglement entropy of a pure state [4], and $R_3 = 2S_3 - 2 \ln 2$. When $L \rightarrow \infty$, we will have $R_3(J \ll J_c, \beta \rightarrow \infty) = R_3(J \gg J_c, \beta \rightarrow \infty) = 0$ for $\rho = \lim_{\beta \rightarrow \infty} e^{-\beta H}/Z$. At the critical point, if the phase transition is driven by large quantum fluctuations and entanglement plays an important role at the critical point, we must observe that R_3 peaks at the critical point. This has been observed in our QMC simulations with $\beta = L$ for the computed system sizes. Therefore, $\beta \sim L$ is still a good choice for simulations.

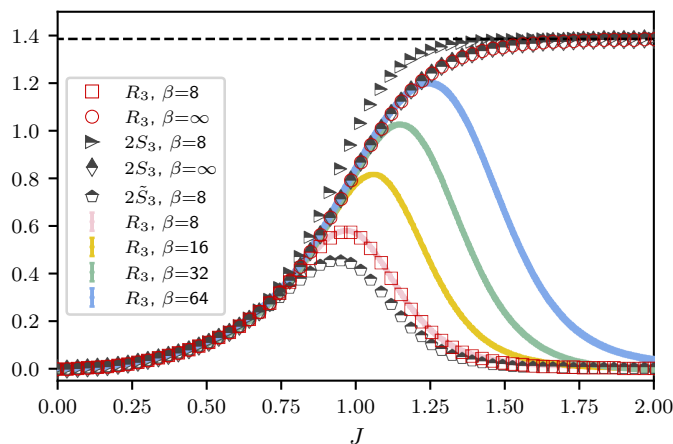


FIG. 2. For the 1D TFIM with $h = 1$, the Rényi negativity R_3 and entanglement Rényi entropy S_3 as functions of J , where the continuous curves are obtained from QMC simulations and the discrete markers represent results obtained from the exact diagonalization method.